





Geometry dependence of excitonic couplings and the consequences for configuration-space sampling

Nils Schieschke¹ | Beatrix M. Bold¹ | Philipp M. Dohmen¹ | Daniel Wehl¹ |
Marvin Hoffmann²  | Andreas Dreuw²  | Marcus Elstner^{1,3}  |
Sebastian Höfener¹ 

¹Institute of Physical Chemistry, Karlsruhe Institute of Technology (KIT), Karlsruhe, Germany

²Interdisciplinary Center for Scientific Computing, Ruprecht-Karls University, Heidelberg, Germany

³Institute of Biological Interfaces (IGB2), Karlsruhe Institute of Technology (KIT), Karlsruhe, Germany

Correspondence

Sebastian Höfener, Institute of Physical Chemistry, Karlsruhe Institute of Technology (KIT), Karlsruhe, Germany.
Email: hoefener@kit.edu

Funding information

Deutsche Forschungsgemeinschaft, Grant/Award Numbers: EL 206/18-1, INST 40/575-1 FUGG (JUSTUS 2 cluster), SFB 1249/Projects B01, B02, B07; Ministerium für Wissenschaft, Forschung und Kunst Baden-Württemberg, Grant/Award Number: bwHPC

Abstract

Excitonic coupling plays a key role for the understanding of excitonic energy transport (EET) in, for example, organic photovoltaics. However, the calculation of realistic systems is often beyond the applicability range of accurate wavefunction methods so that lower-scaling semi-empirical methods are used to model EET events. In the present work, the distance and angle dependence of excitonic couplings of dimers of selected organic molecules are evaluated for the semi-empirical long-range corrected density functional based tight binding (LC-DFTB) method and spin opposite scaled second order approximate coupled cluster singles and doubles (SOS-CC2). While semi-empirically scaled methods can lead to slightly increased deviations for excitation energies, the excitonic couplings and their dependence on the dimer geometry are reproduced. LC-DFTB yields a similar accuracy range as density-functional theory (DFT) employing the ω B97X functional while the computation time is reduced by several orders of magnitude. The dependence of the exchange contributions to the excitonic couplings on the dimer geometry is analyzed assessing the calculation of Coulombic excitonic couplings from monomer local excited states only, which reduces the computational effort significantly. The present work is a necessary first step toward the simulation of excitonic energy transport using semi-empirical methods.

1 | INTRODUCTION

In recent years, organic semiconductors have been widely investigated and applied in electronic and photonic applications.^{1,2} Organic materials are of particular interest for such applications since they combine different desirable properties. They have electronic properties such as low band-gaps that are important for these applications,^{1,3} they are cheap to produce and can be molded in various forms or used as thin films due to their flexibility.^{3,4} For example, systems with conjugated π -systems and aromatic rings have been investigated for their use in organic photovoltaics.^{2,4,5}

To be able to use sunlight as a source for electric energy, light needs to be converted into electric current. Electron donor molecules that are electronically excited transport the absorbed energy to an interface where electric current is generated due to charge separation. This energy transport proceeds without charge-transfer (CT) and is known as excitonic energy transport (EET). In the Frenkel exciton model,⁶ excitons are described via the interactions between excited states, which is also denoted excitonic coupling.⁷ Excitonic couplings have been studied using a wide range of methods^{8–14} ranging from highly accurate to fast, approximate methods. Different classes of molecules and excitonic couplings in different phases have been

This is an open access article under the terms of the Creative Commons Attribution License, which permits use, distribution and reproduction in any medium, provided the original work is properly cited.

© 2021 The Authors. *Journal of Computational Chemistry* published by Wiley Periodicals LLC.

studied.^{2,13,15–17} Recently, density functional theory (DFT) and density functional based tight binding (DFTB) methods have been benchmarked for acenes and small molecules.^{18,19}

In order to assess the performance of different methods, a reference method has to be chosen to meet certain needs. First, results have to be consistent and accurate. Second, the method must not be computationally too expensive, as dimers of systems including multiple aromatic rings need to be feasible. For instance, the second order approximate coupled cluster singles and doubles (CC2) method scales with $\mathcal{O}(N^5)$, which at present means that dimers of pentacene can still be calculated. It is chosen as the reference method since it is an accurate method leading to consistent results for excitation energies compared to CC3.²⁰ The semi-empirically scaled SOS-CC2 is of interest for larger molecular systems since in its Laplace-transformed formalism (LT-SOS-CC2), it scales with $\mathcal{O}(N^4)$, one order of magnitude smaller than CC2.^{21–23}

The algebraic diagrammatic construction (ADC) scheme for the polarization propagator^{24,25} provides a series of ab-initio methods with which excitation energies can be calculated using perturbation theory, following the typical partitioning of the Hamiltonian by Møller and Plesset.²⁶ At second order, ADC(2) provides excitation energies for singles excitations consistent up to second order and their accuracy is very similar to those of CC2.²⁷ However, ADC(2) bares the advantage of being not only size-consistent but also Hermitian.²⁸ In the intermediate-state representation, it provides easy access to excited-state and state-to-state properties.^{29,30} ADC(2) implementations scale formally as $\mathcal{O}(N^5)$, however, with a smaller prefactor than CC2,³¹ while ADC(3) scales formally as $\mathcal{O}(N^6)$.²⁷

DFT is most widely used since it is possible to calculate systems containing more than a hundred atoms routinely. However, results obtained with DFT depend on the employed exchange-correlation functional, and different functionals can result in qualitatively different results. While well-established functionals such as B3LYP have shown to reliably predict some excited-state properties,^{32–35} they show large errors concerning CT processes.^{33,36,37} Because of this, systems with extended conjugation^{38–40} or systems in which CT processes are present are often not described accurately.⁴¹ Improved functionals, such as range-separated functionals that include a long-range correction of the exchange potential, help mitigate this problem.⁴² Long-range corrected (LC) functionals have been tested on their performance with respect to EET processes, where the family of ω B97 functionals has shown to outperform other functionals.⁴³ However, these functionals do not yield a systematic improvement as well, so individual benchmarking is always necessary.

DFTB^{44,45} is an alternative for very large molecular systems, since it is about two to three orders of magnitude faster than DFT using the generalized gradient approximation (GGA) and medium-sized basis sets. It can be derived from DFT using a Taylor series expansion around a reference density, followed by approximations for the two-electron integrals.⁴⁶ Besides these approximations, the accuracy of DFTB is also limited by the applied exchange-correlation functional, which was based on GGA. Only recently, a LC functional has been implemented in the framework of DFTB for the ground

state⁴⁷ and extended to compute excited states properties via the linear-response formalism,⁴⁸ abbreviated LC-DFTB in the following. It has been benchmarked for excitation energies of a large set of organic molecules including charge-transfer excitations.⁴⁸ For the application to exciton-transfer, Coulomb couplings have been investigated.^{49,50} So far, the scheme employed was limited due to the GGA functional used and excitonic couplings in the Coulomb approximation were seemingly only reliable for increased intermolecular distances. Since the calculation of Coulomb couplings is significantly faster, this approach offers the possibility of a further significant gain of computational timings. In the present work, we will address these two aspects in a qualitative manner while no quantitative analysis is attempted, cf. Refs. 51–55. We only aim at addressing the effect of neglecting exchange effects which we measure by comparing the two methods, which was not at hand, for example, in Ref. 50.

The size of molecules used in organic photovoltaics and to be simulated for EET are often so large that computations using wavefunction methods such as CC2, ADC(2), or even standard DFT become unfeasible. In the present work, excitonic couplings obtained with semi-empirical methods are investigated for a selection of organic molecules. We assess the performance by means of the calculation of excited state energies and by the dependence of the couplings on dimer distance and rotation angle. The benchmarking of, for example, excitation energies has been of interest for many years.^{20,56–60}

The article is structured as follows. In Section 2, the methodology and computational details are described. Section 3 contains results obtained for different classes of molecules with the described methods. The work closes with a conclusion.

2 | METHODOLOGY AND COMPUTATIONAL DETAILS

2.1 | Excitonic couplings

The aim of the present work is to assess the accuracy of different electronic-structure methods for the calculation of excitonic couplings J in dimers. Employing supermolecular calculations to study coupled dimers, one immediately can extract the excitation energy difference of two states, $\Delta E_{nm} = E_n - E_m$, where E_m and E_n are defined as the excitation energies of the two interacting states.

Approaching the coupled states from the monomer picture, a two-state model Hamiltonian can be formulated:

$$H = \begin{pmatrix} E_a & J \\ J & E_b \end{pmatrix}, \quad (1)$$

where E_a and E_b denote excitation energies for local excited (diabatic) states on monomers A and B, respectively. Analytical diagonalization of this 2×2 matrix yields the excitation energies of the (adiabatic) dimer states E_m and E_n , and their difference is given as:

$$\Delta E_{nm} = 2\sqrt{\frac{1}{4}\Delta E_{ab}^2 + J^2}. \quad (2)$$

Re-arranging Equation (2) shows the influence of the energy difference ΔE_{nm} upon the excitonic coupling J :

$$J(m, n) = \frac{1}{2}\sqrt{\Delta E_{nm}^2 - \Delta E_{ab}^2}. \quad (3)$$

In case of symmetric dimers, that is, $\Delta E_{ab} = 0$, the coupling J simplifies to:

$$J(m, n) = \frac{1}{2}\Delta E_{nm}. \quad (4)$$

The difference ΔE_{nm} obtained from supermolecular calculations, however, does not correspond precisely to the target coupling $J(m, n)$ of the two states in general. Equation (4) is valid thus only in the two-state model, c.f. Refs. 61,62 that means if no significant mixing with further states occurs, which is assumed in the present work.

The pure Coulomb coupling^{49,50} of two local excited states a and b on molecules A and B , respectively, can be calculated in a tight-binding framework using TD-DFTB as

$$J_C(a, b) = \sum_{X \in A} \sum_{Y \in B} Q_X^{0a} \zeta_{XY} Q_Y^{0b}, \quad (5)$$

where X and Y are the atoms of the corresponding molecules. Q^{0a} and Q^{0b} are the atomic Mulliken transition charges for the excited states a and b , respectively. The pure atomic Coulomb interaction ζ_{XY} is defined as

$$\zeta_{XY} = \iint \frac{\Phi_X(\mathbf{r})\Phi_Y(\mathbf{r}')}{|\mathbf{r} - \mathbf{r}'|} d\mathbf{r} d\mathbf{r}' \quad (6)$$

where

$$\Phi_X(\mathbf{r}) = \frac{1}{N_X} \sum_{\mu \in X} |\mu(\mathbf{r})|^2, \quad (7)$$

in which $\mu(\mathbf{r})$ denote basis functions and N_X is the total number of basis functions on atom X . ζ_{XY} can be calculated analogously to the electron-electron interaction term γ_{XY} in the LC-DFTB formalism.⁴⁷ For further details of this approach the reader is referred to Ref 49.

If the coupling obtained from supermolecular excited states m and n (Equation (4)) is in sufficient agreement with the Coulomb coupling of two local states a and b according to Equation (5), that is $J(m, n) \approx J_C(a, b)$, then exchange effects are negligible. Note, however, that the Mulliken transition charges in Equation (5) are an additional approximation so that even for increased distances small deviations may remain, vide infra. As the calculation of $J_C(a, b)$ is significantly faster compared to $J(m, n)$, using only the former would provide a

computational significant advantage in the simulation of large molecular systems.

2.2 | Geometries

The dimers required for the study of interacting local states were constructed by optimizing the geometries of the monomers with B3LYP and stacking two monomers symmetrically face to face. In bulk material, however, relative positions between monomers differ by, for example, intermolecular distance and rotation angle (Figure 1). The distances at which the excitation energies are calculated are thus chosen as $r = \{3.5, 4.0, 5.0, 6.0\}$ Å. Additionally, the rotation angles φ of 30°, 60° and 90° were studied at fixed 4.0 Å distance.

In the following, two sets of molecules are discussed separately: First set A, consisting of different acenes and then, set B, consisting of guanine and purine as well as different naphthyridines (Figure 2) in order to assess the influence of nitrogen substitution effects.

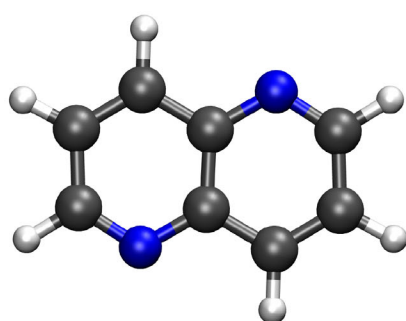
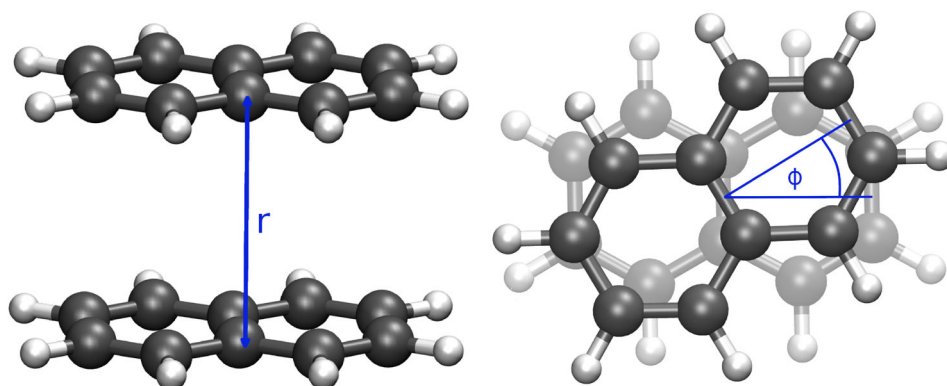
2.3 | Electronic-structure methods

All calculations employing CC2, SCS-CC2 and SOS-CC2 were carried out using the TURBOMOLE program^{63–65} and the def2-TZVPPD basis. ADC(2) and ADC(3) calculations were carried out using the TURBOMOLE program and Q-Chem 5.1⁶⁶ employing a def2-SVPD basis, c.f. Supporting Information.

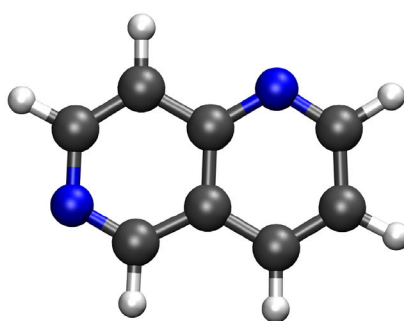
Supermolecular calculations using the LC functional ω B97X were performed with the ORCA program package.⁶⁷ The Tamm-Dancoff approximation (TDA) has been used in combination with the resolution of the identity (RI) approximation. The def2-TZVP basis set is employed in combination with semi-numeric exact exchange, and RI-J is used for the Coulomb contribution together with the def2/J auxiliary basis set.

In LC-DFTB the local BNL functional^{68,69} was used for the short-range part and a conventional non-local Hartree-Fock exchange for $\omega \rightarrow \infty$ for the long-range part.⁴⁸ The range-separation parameter ω is set to $\omega = 0.3/a_0$ for the computation of the electronic parameters.⁴⁸ DFTB uses a minimal atomic orbital basis set, which is computed from atomic Kohn-Sham equations, and an additional harmonic potential is introduced to confine the basis function. The harmonic potential is characterized by confinement radii r_0 , which determine the range of the potential and therefore the extension of the LCAO basis functions. The radii r_0 are usually optimized for properties such as atomization energies, geometries and vibrational frequencies of molecules, resulting typically in values being a factor of 2 of the covalent radii of the corresponding atoms.⁴⁵ The original LC-DFTB confinement radii lead to accurate vertical excitation energies and Coulomb couplings employing rather compact atomic orbital basis sets.⁴⁸ Such a confined basis, however, leads to underestimated electron-transfer couplings,¹⁸ as this property is based on exchange for which diffuse basis functions are required to properly describe the overlap of the fragment wavefunctions. As the intermolecular distance decreases, overlap and exchange effects increase, leading to increased errors for the confined

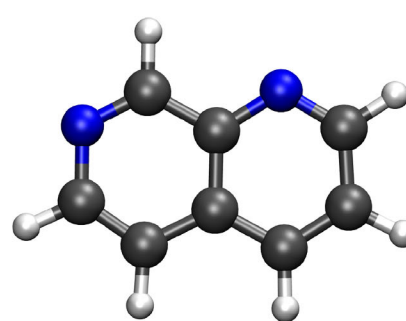
FIGURE 1 Definition of the distance r and the rotation angle φ at the example of naphthalene



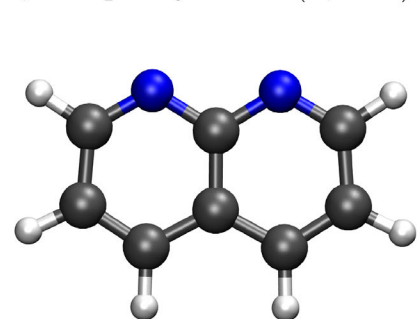
1,5-Naphthyridine (1,5-N.)



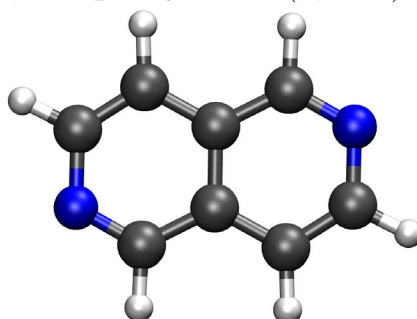
1,6-Naphthyridine (1,6-N.)



1,7-Naphthyridine (1,7-N.)



1,8-Naphthyridine (1,8-N.)



2,6-Naphthyridine (2,6-N.)

FIGURE 2 Naphthyridines of set B

basis and different choices of the confinement radii need to be assessed, c.f. Supporting Information. Selected parameter sets investigated are compiled in the Supporting Information. In the following, we use one set of radii with confined atomic orbitals for excitation energies, denoted “parameter set 1,” and a second set of optimized radii for the calculation of the coupling J , denoted “parameter set 2,” c.f. Supporting Information.

2.4 | Method assessment

Due to the size of the dimer systems and the large amount of distances and angles, we have chosen to use CC2 as general benchmark method. However, as CC2 is only a second-order method, its accuracy is briefly assessed with respect to ADC(3). For the present purpose excitation energies and supermolecular couplings at selected

distances and angles of pyrrol, pyridine, and pyrazine dimers are compared, see Table 1, where the excitonic coupling is given as $J = \frac{1}{2}(E_2 - E_1)$. For the investigated properties ADC(3) and CC2 yield practically identical results. For example, the couplings J obtained with LC-DFTB yield a mean error of +9 meV and standard deviation of 25 meV with respect to ADC(3) and a mean error of +7 meV and a standard deviation of 21 with respect to CC2, respectively. Based on these results and the small deviations between ADC(3) and CC2, we will evaluate SOS-CC2 and SCS-CC2 with respect to CC2.

2.5 | Sampling

For sampling, a large number of dimer geometries were taken from molecular dynamics (MD) simulations of an anthracene crystal containing $10 \times 40 \times 5$ molecules along the respective crystallographic

TABLE 1 Excitation energies E_1 and E_2 belonging to states S_1 and S_2 , respectively, in eV and couplings J in meV of a set of small dimers at selected distances and angles φ . Oscillator strengths f in parentheses in units of 10^{-3}

Molecule	φ	ADC(3)			CC2			ω B97X			LC-DFTB		
		r	E_1		J	E_2		E_1	J	E_2	E_1^e	E_2^e	f^f
			E_1	E_2		E_1	E_2						
Pyrrol	0	3.5	4.800 (0)	5.302 (12)	251	4.839 (0)	5.373 (10)	6.267 (0)	267	6.962 (15)	6.394 (0)	6.542 (184)	353
		4.0	5.064 (0)	5.306 (4)	121	5.131 (0)	5.386 (2)	6.607 (0)	128	6.962 (343)	6.439 (0)	6.530 (193)	142
		5.0	5.264 (0)	5.318 (0)	27	5.358 (0)	5.414 (0)	6.807 (0)	28	6.910 (372)	6.466 (0)	6.513 (205)	39
Pyrrol	180	6.0	5.337 (0)	5.351 (0)	7	5.441 (0)	5.456 (0)	6.857 (0)	7	6.908 (393)	6.478 (0)	6.506 (212)	18
		3.5	5.060 (0)	5.333 (8)	137	5.092 (0)	5.388 (6)	6.330 (0)	148	6.884 (266)	6.450 (0)	6.533 (167)	129
		4.0	5.261 (0)	5.410 (6)	75	5.324 (0)	5.489 (5)	6.683 (0)	82	6.916 (303)	6.471 (0)	6.528 (181)	60
Pyridine	0	5.0	5.367 (0)	5.408 (1)	21	5.459 (0)	5.503 (1)	6.828 (0)	22	6.910 (360)	6.482 (0)	6.516 (199)	26
		6.0	5.397 (0)	5.410 (0)	6	5.500 (0)	5.513 (0)	6.855 (0)	7	6.908 (349)	6.487 (0)	6.508 (208)	16
		3.5	4.771 (0)	5.135 (46)	182	4.996 (0)	5.375 (40)	5.475 (0)	190	5.790 (56)	5.636 (0)	5.676 (40)	212
Pyridine	180	4.0	4.999 (0)	5.125 (50)	63	5.244 (0)	5.368 (44)	5.630 (0)	62	5.779 (63)	5.653 (0)	5.673 (44)	76
		5.0	5.089 (0)	5.116 (57)	14	5.338 (0)	5.362 (51)	5.733 (0)	12	5.774 (72)	5.657 (0)	5.669 (50)	17
		6.0	5.102 (0)	5.115 (60)	6	5.352 (0)	5.362 (54)	5.753 (0)	5	5.767 (77)	5.659 (0)	5.666 (53)	9
Pyridine	180	3.5	4.812 (0)	5.139 (44)	163	5.044 (0)	5.382 (38)	5.534 (0)	169	5.792 (53)	5.639 (0)	5.676 (39)	171
		4.0	5.019 (0)	5.130 (49)	55	5.265 (0)	5.374 (43)	5.652 (0)	54	5.781 (60)	5.654 (0)	5.673 (43)	54
		5.0	5.095 (0)	5.119 (56)	12	5.344 (0)	5.366 (50)	5.749 (0)	11	5.777 (71)	5.658 (0)	5.669 (49)	15
Pyrazine	0	6.0	5.105 (0)	5.117 (60)	6	5.355 (0)	5.365 (54)	5.755 (0)	5	5.767 (76)	5.660 (0)	5.667 (52)	9
		3.5	4.598 (0)	5.021 (137)	211	4.866 (0)	5.274 (116)	5.254 (0)	204	5.776 (184)	5.642 (0)	5.696 (128)	193
		4.0	4.819 (0)	5.001 (147)	91	5.086 (0)	5.254 (128)	5.523 (0)	84	5.751 (204)	5.627 (0)	5.686 (139)	98
ADC(3)	reference	5.0	4.913 (0)	4.975 (163)	31	5.178 (0)	5.232 (144)	5.597 (0)	27	5.714 (226)	5.639 (0)	5.673 (153)	32
		6.0	4.934 (0)	4.966 (171)	16	5.197 (0)	5.224 (153)	5.671 (0)	14	5.708 (239)	5.645 (0)	5.665 (160)	18
		ME ^a	+0.180	+0.183	+1	+0.988	+1.008	+0.932	+10	+0.823	+0.823	+9	
CC2	reference	STD ^b	0.089	0.081	6	0.391	0.425	0.312	44	0.287	0.287	24	
		MAE ^c	0.180	0.183	4	0.988	1.008	0.932	31	0.823	0.823	14	
		MA ^d	0.268	0.259	16	1.543	1.657	1.594	140	1.240	1.240	102	
reference	MAE ^c	ME ^a	+0.807	+0.825	+9	+0.751	+0.640	+0.751	+9	+0.640	+0.640	+7	
		STD ^b	0.475	0.503	44	0.394	0.366	0.394	44	0.366	0.366	21	
		MAE ^c	0.807	0.825	32	0.751	0.640	0.751	32	0.640	0.640	13	
reference	MA ^d	MAE ^c	1.476	1.576	129	1.555	1.169	1.555	129	1.169	1.169	85	

^aMean error.
^bStandard deviation.
^cMean absolute error.
^dMaximum absolute error.
^eParameter set 1 (confined AO's).
^fParameter set 2 (optimized AO's).

axes a , b and c .⁷⁰ For use in the present work, one anthracene pair in the crystallographic b -direction in the center of the crystal was extracted from the MD snapshots, as pairs along this direction show the highest coupling values.

Exciton diffusion constants were calculated using a master equation (MEQ) approach, which was solved stochastically for a single exciton using kinetic Monte Carlo simulations.^{71,72} Transfer rates were determined according to Marcus theory as:^{73,74}

$$k_{ij} = \frac{J^2}{\hbar} \sqrt{\frac{\pi}{k_B T \lambda}} \exp\left(-\frac{\lambda}{4 k_B T}\right), \quad (8)$$

with a reorganization energy λ of 0.563 eV⁷⁰ and the coupling J . For the crystal structure (static) the coupling value J is taken directly, while for sampled structures (dynamic) the root mean square (RMS) value J_{RMS} ,⁷⁵

$$J_{\text{RMS}} = \sqrt{\langle J^2 \rangle} = \sqrt{\langle J \rangle^2 + \sigma^2}, \quad (9)$$

is used, where σ is the standard deviation. The latter accounts for fluctuations around the average structure.

A value to quantify the degree of influence of the dynamics is the coherence parameter,^{75,76}

$$C = \frac{\langle J \rangle^2}{\langle J^2 \rangle} = \frac{1}{1 + \frac{\sigma^2}{\langle J \rangle^2}}, \quad (10)$$

reaching values near 1 or 0 when the coupling is defined by the average structure or by non-equilibrium conformations, respectively. The mean-square displacement (MSD) of the exciton averaged over 10,000 trajectories (N_{traj}) is calculated as:⁷⁷

$$\text{MSD}(t) = \frac{1}{N_{\text{traj}}} \sum_I \sum_A^{N_{\text{traj}}} (x_A^I(t) - x^I(0))^2 p_A^I(t), \quad (11)$$

where $x_A^I(t)$ is the center of mass of molecule A along trajectory I , $p_A^I(t)$ is the corresponding diabatic population and $x^I(0)$ is the center of the exciton at the start of the simulation ($t = 0$). The diffusion constant D was finally calculated as follows:

$$D = \frac{1}{2} \lim_{t \rightarrow \infty} \frac{d \text{MSD}(t)}{d t}. \quad (12)$$

In case of the model dimer systems the coupling can be obtained as half the energy difference of the coupled states, c.f. Figure 3. The underlying condition is, however, that the two monomers have identical geometries and thus degenerate excited states, so that Equation (4) can be used. In case of the MD simulation the two monomers are no longer identical and do not possess degenerate excitation energies so that Equation (3) has to be used. To obtain the individual monomer

energies, for each snapshot not only the dimers have to be calculated but also the individual monomers using the parameter set 2 optimized for coupling. It must be pointed out, however, that despite using Equation (3) still numerical problems can occur. If the excitation energy gap of the dimer is smaller than the difference of monomer excitation energies, the square-root term becomes negative and the coupling becomes imaginary. This problem may be rooted in the approximate nature of the overall approach, which assumes that the dimer states are a linear combination of the two corresponding monomer states only. However, only a small amount of about 0.5% of the couplings turned out to be imaginary and the corresponding snapshots were neglected for the analysis.

3 | RESULTS

The results are ordered as follows. We begin by assessing the performance of the different electronic-structure methods for model dimers of set A, followed by an analogous investigation for the model dimers of set B. For set A, additionally Coulomb couplings are discussed, i.e. a qualitative estimate of the influence of exchange contributions for different dimer geometries. Finally, anthracene is investigated in a realistic crystal geometry to also study structural influences beyond the intermolecular distance and angle dependence.

3.1 | Model dimers: Set A

3.1.1 | Excitation energies

We start with the assessment of the accuracy of absolute excitation energies obtained with the different methods. In the present work, S_1 and S_2 label the two interacting states, of which S_1 is the state with small or zero oscillator strength and S_2 exhibits a large oscillator strength. Provided Equation (4) can be used, excitonic couplings are given in the present work as $J = \frac{1}{2}(E_2 - E_1)$, where E_1 and E_2 belong to the states S_1 and S_2 , respectively. In the uncoupled regime, the states S_1 and S_2 are degenerate.

Individual results for the molecules are given in the Supporting Information. In Tables 2 and 3 errors of excitation energies are collected for set A, computed using different electronic-structure methods. The tables reveals that ADC(2), using the def2-SVPD basis, yields energies approximately 0.1 eV higher than CC2, using the def2-TZVPPD basis. This deviation is dominated by the basis-set incompleteness error (BSIE). Nevertheless, the low value of the standard deviation (STD) of 0.01 eV shows that results obtained using ADC(2)/def2-SVPD are consistently shifted compared to CC2/def2-TZVPPD.

SCS-CC2 and SOS-CC2 yield excitation energies approximately 0.2–0.3 eV higher compared to CC2. Although the triple-zeta basis def2-TZVPPD is used, both ME and MA are considerably higher compared to using ADC(2) with the smaller basis set. The standard deviation (STD) of SCS- and SOS-CC2 reveals that their results are less

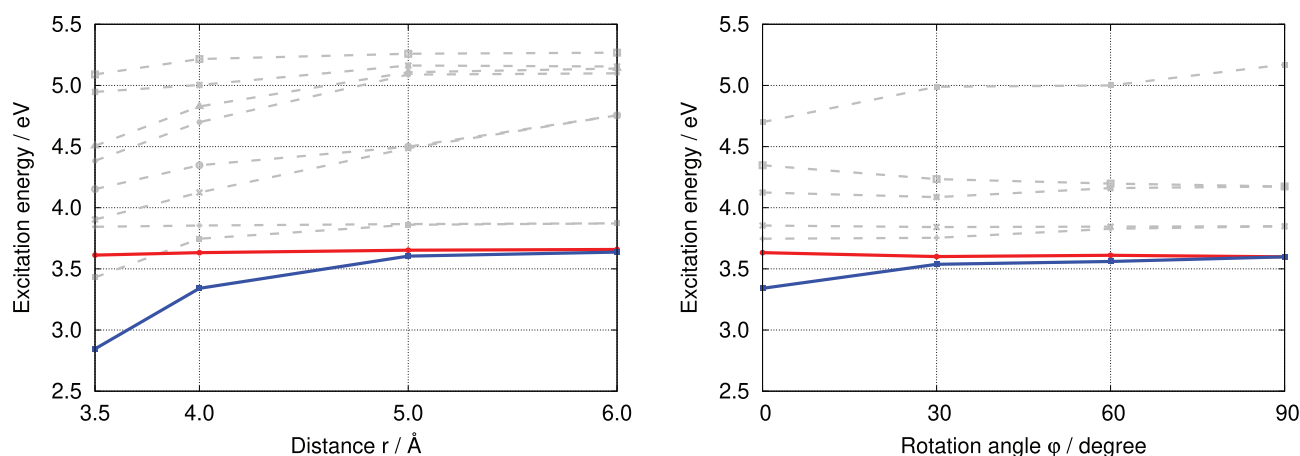


FIGURE 3 The first 10 excitation energies of the anthracene dimer calculated using CC2 for selected intermolecular distances at 0° angle (left) and different angles at constant 4.0 Å distance (right). Excitonically coupled states are drawn in thick lines. E_1 (blue) is the lower (dark) state which depends significantly upon the dimer geometry. E_2 (red) is the upper (bright) state which is almost independent of the dimer geometry

TABLE 2 Errors in eV of the excitation energies E_1 and E_2 belonging to states S_1 and S_2 , respectively, compared to results obtained using CC2 of set A summed over all investigated distances r and angle $\varphi = 0^\circ$

	ADC(2)		SCS-CC2		SOS-CC2		ω B97X		LC-DFTB ^e	
	E_1	E_2	E_1	E_2	E_1	E_2	E_1	E_2	E_1	E_2
ME ^a	+0.074	+0.075	+0.196	+0.184	+0.275	+0.254	+0.358	+0.407	+0.071	−0.118
STD ^b	0.010	0.011	0.057	0.045	0.093	0.082	0.074	0.093	0.334	0.200
MAE ^c	0.074	0.075	0.196	0.184	0.275	0.254	0.358	0.407	0.267	0.193
MA ^d	0.093	0.093	0.311	0.269	0.439	0.365	0.520	0.596	0.793	0.416

^aMean error.

^bStandard deviation.

^cMean absolute error.

^dMaximum absolute error.

^eParameter set 1 (confined AO's).

TABLE 3 Errors in eV of the excitation energies E_1 and E_2 belonging to states S_1 and S_2 , respectively, compared to results obtained using CC2 of set A at $r = 4$ Å and summed over all investigated angles

	ADC(2)		SCS-CC2		SOS-CC2		ω B97X		LC-DFTB ^e	
	E_1	E_2	E_1	E_2	E_1	E_2	E_1	E_2	E_1	E_2
ME ^a	+0.071	+0.072	+0.190	+0.184	+0.281	+0.270	+0.365	+0.398	−0.050	−0.099
STD ^b	0.010	0.011	0.039	0.040	0.059	0.062	0.061	0.079	0.191	0.182
MAE ^c	0.071	0.072	0.190	0.184	0.281	0.270	0.365	0.398	0.164	0.175
MA ^d	0.087	0.088	0.278	0.246	0.410	0.365	0.471	0.537	0.363	0.383

^aMean error.

^bStandard deviation.

^cMean absolute error.

^dMaximum absolute error.

^eParameter set 1 (confined AO's).

consistent compared to those of ADC(2). SCS-CC2 and SOS-CC2 are semi-empirically scaled flavors of CC2. SCS-CC2 does not provide a reduced computational effort, while the SOS-CC2 method exhibits a scaling of the computational effort with number of basis functions

N that can be reduced by one order of magnitude, that is, $\mathcal{O}(N^4)$ instead of $\mathcal{O}(N^5)$ when the Laplace transformation is used.^{21–23}

TDDFT employing the range-separated ω B97X functional yields excitation energies which are 0.3–0.4 eV higher than those obtained

with CC2. However, the STD of somewhat below 0.1 eV and a maximum error of 0.56 to 0.6 eV show an increased error distribution compared to the scaled wavefunction methods. The agreement of mean error and mean absolute error shows that the excitation energies are systematically overestimated.

The LC-DFTB values in Tables 2 and 3 were obtained using parameter set 1, that is, with confined AOs, vide supra. The mean deviations seem to be small but the standard deviation shows that excitation energies are both overestimated and underestimated to a similar extent, the overall accuracy is comparable to that of LC-DFT.

3.1.2 | Excitonic couplings: Distance dependence

Having addressed the accuracy of the excitation energies, we now turn to excitonic couplings and, in particular, their dependence on intermolecular distances and angles. For example, in Figure 3 the excitation energies are displayed in the face-to-face oriented anthracene dimer for selected distances and angles. The investigated excitonic couplings are displayed in this figure as non-dashed, thick lines. The pair of excitations that represents the excitonic coupling has two properties: While the higher excitation energy, denoted E_2 in the present work, shows no or only minor dependency on the distance r , the lower excitation energy, denoted E_1 in the present work, does depend significantly on the distance r . Furthermore, E_2 has a nonzero oscillator strength whereas E_1 has an oscillator strength of zero for $\varphi = 0$. The couplings as obtained in this manner are discussed in the following.

Results for set A are collected in Table 4. In this table, the reference values of the CC2 method are displayed as absolute coupling values while the couplings obtained with the other methods are given relative to the CC2 value. Additionally, the deviations given in the table are displayed as correlation plots in Figure 4. The table reveals that ADC(2) has a mean error of about +0.08 eV in case of absolute excitation energies, while the mean error of the couplings J is less than 1 meV. The performance of a method with respect to excitation energies does therefore not necessarily directly translate to its performance for predicting excitonic couplings as long as the electronic structure of the state is sufficiently accurately described.

In case of the scaled CC2 variants, SCS-CC2 and SOS-CC2, the mean errors of the coupling are slightly increased compared to ADC(2)/def2-SVPD. In particular the standard deviation and the maximum errors are increased by one order of magnitude for the absolute (and relative) errors. In case of DFT and LC-DFTB the errors are again somewhat increased. LC-DFTB shows a better accuracy than DFT employing the ω B97X functional. Note, however, that in case of DFTB the couplings must be computed with a different parameter set than the absolute excitation energies. The observed deviations are overall small compared to the absolute coupling strength, so that different decay rates are within the margin of error. For example, plotting the distance dependence of total couplings will exhibit no visible effect, cf. the analysis for naphthyridines in Figure 9. As LC-DFTB and

ω B97X show deviations from CC2 in a similar range which we expect for other DFT-functionals as well, we decided not to further interpret these differences.

3.1.3 | Excitonic couplings: Rotation-angle dependence

Results for the dependence of the couplings on the rotation angle are also collected in Table 4, and displayed for the reference method CC2 in Figure 5. While in most cases the coupling decreases from 0° to 90° steadily, naphthalene and pyrene exhibit a minimum in the coupling at 30° and a maximum at 60°, cf. Section 3.1.4. The coupling strengths at 60° decrease with increasing length of the linear acenes, that is, from naphthalene to pentacene. With increasing chain length, however, the couplings at 30° and 90° remain almost unchanged, so that only naphthalene shows a local maximum while for anthracene to pentacene a steady decrease from 0° to 90° is observed.

3.1.4 | Coulomb couplings

The calculation of Coulomb couplings is computationally very efficient because they are available from monomer calculations and no wavefunction overlap has to be computed. To avoid supermolecular calculations it might thus be tempting to approximate excitonic couplings as Coulomb couplings. In the following, it is addressed in which cases this approximation is numerically accurate and thus justified at the example of set A.

A comparison of Coulomb couplings and supermolecular excitonic couplings is shown Figure 6 for varying distance at a constant rotation angle of $\varphi = 0^\circ$. The figure reveals that exchange effects are observable below 5 Å. At around 4 Å they are significant and at around 3.5 Å they dominate the coupling for the investigated coupled states. As a consequence, Coulomb couplings yield smaller values than excitonic couplings.

For larger distances, starting from 5 to 6 Å, the LC-DFTB Coulomb couplings are larger than the supermolecular couplings, which is unexpected, since for large distances the exchange contributions should vanish, and both computation approaches are expected to lead to the same values. Taking the supermolecule couplings as a reference, it seems that LC-DFTB Coulomb couplings are slightly overestimated. This might be due to the approximations involved in the calculation of the Coulomb couplings, such as Mulliken charges computed within the DFTB minimal basis set or the properties of the response vectors, which can lead also to too large oscillator strengths,⁴⁸ for example.

In Figure 7, a comparison of excitonic couplings, i.e. supermolecular calculations, and Coulomb couplings for varying rotation angle at a constant distance of $r = 4$ Å is shown. Note that the values at 0° are precisely those in Figure 6 at distance $r = 4$ Å. While for 0° the amount of exchange leads to a clear deviation of

TABLE 4 Excitonic couplings in meV for set A. The values for CC2 are given as absolute coupling strength, while the other methods' results are given relative to the CC2 values

		CC2	ADC(2)	SCS- CC2	SOS- CC2	ω B97X	LC-DFTB ^e		CC2	ADC(2)	SCS- CC2	SOS- CC2	ω B97X	LC-DFTB ^e
Naphthalene	3.5	367	+2	-39	-60	-9	-11	0	135	+1	-18	-27	+0	-8
	4	135	+1	-18	-27	+0	-8	30	27	-0	-6	-10	-3	+11
	5	23	-0	-1	-2	+7	+5	60	39	+1	-7	-11	-3	+16
	6	10	-0	-0	-0	+3	+6	90	0	+0	-0	-0	-0	+0
Anthracene	3.5	383	+2	-31	-47	+20	+7	0	146	+1	-16	-23	+20	+6
	4	146	+1	-16	-23	+20	+6	30	32	+0	-3	+1	+22	+19
	5	24	-0	+2	+3	+11	+12	60	25	+1	+3	-5	+15	+10
	6	11	+0	+2	+3	+11	+10	90	0	-0	-0	-0	+0	+0
Tetracene	3.5	392	+2	-26	-41	+38	+10	0	154	+1	-16	-22	+32	+10
	4	154	+1	-16	-22	+32	+10	30	30	+4	+4	+6	+37	+25
	5	24	-0	+3	+5	+18	+16	60	20	+1	+3	+4	+22	+21
	6	11	-0	+3	+4	+17	+13	90	0	+0	+0	+0	+0	+0
Pentacene	3.5	396	+3	-21	+0	+54	+9	0	161	+0	-16	-23	+41	+11
	4	161	+0	-16	-23	+41	+11	30	27	+0	+7	+10	+46	+28
	5	24	-0	+4	+6	+24	+18	60	15	+1	+4	+6	+27	+16
	6	11	-0	+4	+5	+21	+14	90	0	+0	+0	+0	+0	+0
Benzanthracene	3.5	285	+6	+27	+25	+81	+80	0	111	+6	+7	-1	+37	+21
	4	111	+6	+7	-1	+37	+21	30	15	+2	+6	+5	+4	+22
	5	18	+0	+2	+2	+33	+12	60	12	+0	-0	-1	+3	+8
	6	8	+0	+2	+2	+36	+10	90	4	+0	-0	-0	+3	+0
Perylene	3.5	436	+1	-19	-32	+38	-6	0	206	-2	-15	-22	+33	+17
	4	206	-2	-15	-22	+33	+17	30	66	-0	+8	+11	+50	+42
	5	63	-1	+3	+5	+33	+25	60	14	-0	+11	+15	+35	+13
	6	39	-1	+4	+5	+25	+22	90	0	+0	-0	-0	-0	+0
Pyrene	3.5	379	-4	+24	-1	+57	+39	0	199	-2	-28	-43	-3	+12
	4	199	-2	-28	-43	-3	+12	30	46	+1	-0	-3	+51	+31
	5	54	-1	-3	-6	+2	+16	60	95	-1	-11	-18	-8	+19
	6	32	-0	-1	-3	+6	+14	90	0	+0	+0	+0	+0	+0
ME ^a			±0	-6	-10	+24	+14			±0	-3	-5	+16	+13
STD ^b			2	15	20	20	16			1	9	13	19	11
MAE ^c			1	12	15	25	16			1	7	9	18	13
MA ^d			6	39	60	81	80			6	28	43	51	42

^aMean error.^bStandard deviation.^cMean absolute error.^dMaximum absolute error.^eParameter set 2 (optimized AO's).

excitonic and Coulomb couplings, this deviation vanishes for increased angles and is significantly reduced already at 30° rotation. Figure 7 reveals that the angle has a significant impact not only on the coupling strength, c.f. Table 4, but apparently also on the wavefunction overlap, that is, the exchange contribution. A similar behavior might also be expected for displacements and tilting, as occurring in Section 3.3. For naphthalene and pyrene, however, the supermolecular couplings

exhibit local minima at 30° and local maxima at 60°, which are also observed for the reference methods, cf. Figure 5, implying that the exchange strength depends on the relative geometries in a non-trivial manner. Therefore, Coulomb couplings can be a good approximation to excitonic couplings even at small intermolecular distances, since exchange effects depend sensitively on the geometric configuration. Indeed, this seems to be the case in the anthracene crystal, vide infra.

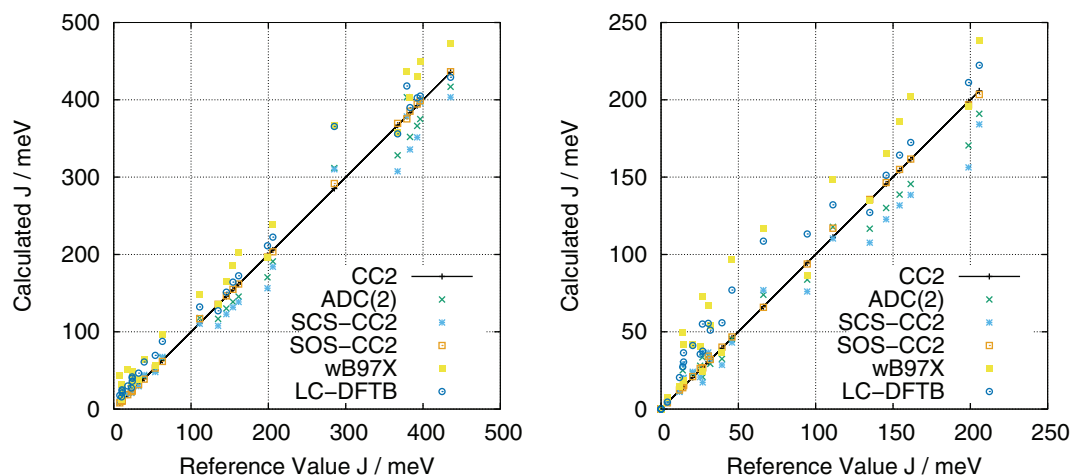


FIGURE 4 Correlation plots of excitonic couplings in case of distances (left) and angles (right) for set A. Note that the plot of the angles has only half the range of the distance plot

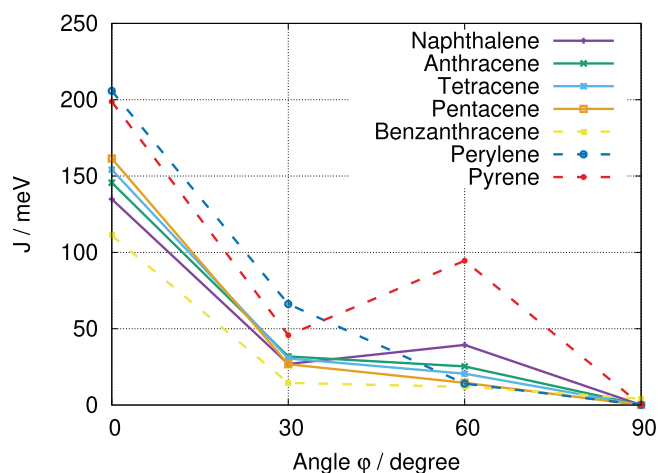


FIGURE 5 Angle dependence of excitonic couplings J in meV, calculated using CC2 for set A at $r = 4 \text{ \AA}$

3.2 | Model dimers: Set B

In this section, the objective is to examine how the different position of nitrogen substitutions can influence the excitonic couplings. For this, purine and guanine as well as five different naphthyridines as shown in Figure 2 were investigated.

3.2.1 | Excitation energies

Analogously to set A, we start with the assessment of the accuracy of the original excitation energies obtained with the different methods. In Tables 5 and 6 excitation energies are collected for set B. In general, it is observed that compared to set A, the errors are more homogeneous due to the similarity of the naphthyridines.

The table reveals that ADC(2), using the def2-SVPD basis, leads to energies about 0.03 eV lower than CC2, using the def2-TZVPPD basis. The standard deviation, however, is approximately somewhat below 0.2 eV. SCS-CC2 leads to a mean absolute error of about 0.06 eV and an STD of 0.07 eV. In case of SOS-CC2, a mean absolute error of 0.09 eV and a STD of about 0.1 eV is obtained. The values for the semi-empirically scaled variants employing the def2-TZVPPD basis are in the same order of magnitude as ADC(2) employing the def2-SVPD basis.

Results calculated using the ω B97X functional show a ME of about +0.3 – +0.4 eV and a STD somewhat below 0.2 eV. The value of the STD being significantly smaller than that of the ME shows that for set B ω B97X results in consistent errors for excitation energies compared to CC2, certainly due to the choice of molecules. LC-DFTB results exhibit a mean absolute error of about 0.1 eV to 0.2 eV, a STD of about 0.2 eV, and a maximum error of 0.464 eV.

3.2.2 | Excitonic couplings

In Table 7, couplings calculated using different methods are compared to couplings calculated using CC2. In this table, the reference values of the CC2 method are displayed as absolute coupling values while the couplings obtained with the other methods are given relative to the CC2 value. Additionally, the deviations given in the table are displayed as correlation plots in Figure 8.

ADC(2) results in a ME of –7 meV, an STD of 10 meV and a maximum deviation of 42 meV for varying distance. In case of varying angle, the mean error is found to be –31 meV and an STD of 28 meV. The maximum error is as large as 100 meV. It should be pointed out that for the angle dependence relative errors are quite large for all methods as the coupling values are in general small.

SCS-CC2 shows a ME of –10 meV and a maximum deviation of 40 meV. The STD of about 10 meV shows that using SCS-CC2 leads

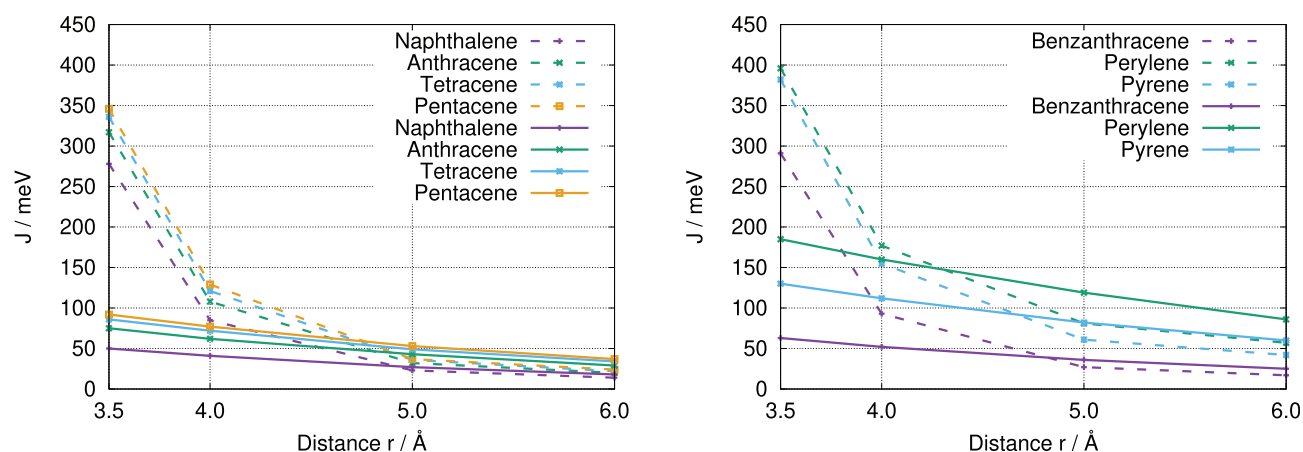


FIGURE 6 Excitonic couplings (dashed lines) and Coulomb couplings (solid lines) with varying distance at a constant angle of $\varphi = 0^\circ$ computed using LC-DFTB, divided into linear (left) and non-linear (right) acenes

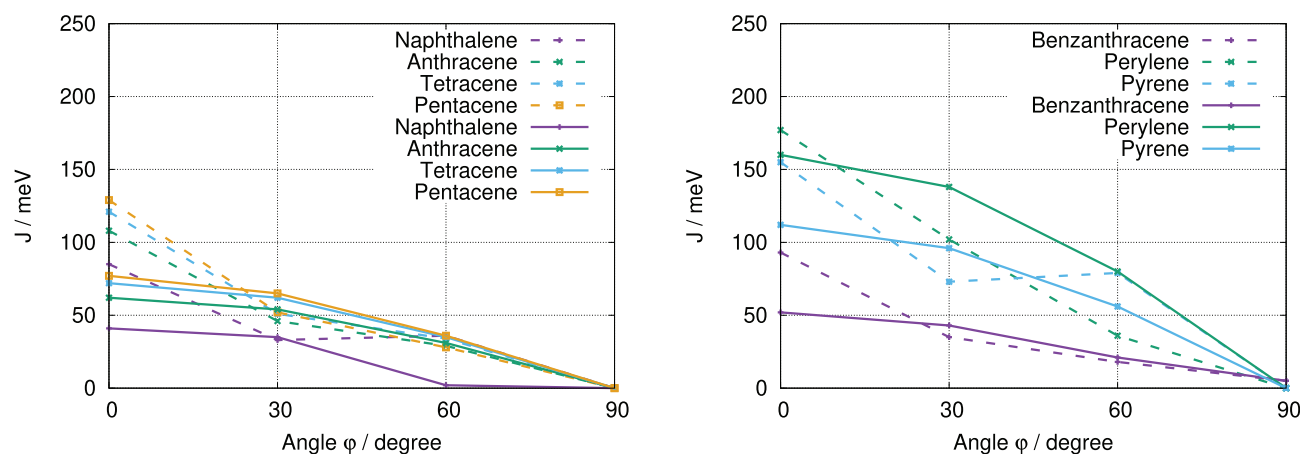


FIGURE 7 Excitonic couplings (dashed lines) and Coulomb couplings (solid lines) with varying rotation angle at a constant distance of $r = 4 \text{ Å}$ computed using LC-DFTB, divided into linear (left) and non-linear (right) acenes

TABLE 5 Errors in eV of the excitation energies E_1 and E_2 belonging to states S_1 and S_2 , respectively, compared to results obtained using CC2 of set B summed over all investigated distances r and angle $\varphi = 0^\circ$

	ADC(2)		SCS-CC2		SOS-CC2		ω B97X		LC-DFTB ^e	
	E_1	E_2	E_1	E_2	E_1	E_2	E_1	E_2	E_1	E_2
ME ^a	−0.021	−0.034	+0.011	−0.010	+0.011	−0.019	+0.318	+0.335	+0.064	−0.024
STD ^b	0.182	0.185	0.074	0.070	0.111	0.101	0.186	0.184	0.215	0.167
MAE ^c	0.119	0.117	0.062	0.064	0.093	0.095	0.350	0.366	0.160	0.102
MA ^d	0.490	0.489	0.170	0.117	0.262	0.159	0.606	0.500	0.464	0.451

^aMean error.

^bStandard deviation.

^cMean absolute error.

^dMaximum absolute error.

^eParameter set 1 (confined AO's).

TABLE 6 Errors in eV of the excitation energies E_1 and E_2 belonging to states S_1 and S_2 , respectively, compared to results obtained using CC2 of set B at $r = 4$ Å and summed over all investigated angles

	ADC(2)		SCS-CC2		SOS-CC2		ω B97X		LC-DFTB ^e	
	E_1	E_2	E_1	E_2	E_1	E_2	E_1	E_2	E_1	E_2
ME ^a	−0.027	−0.035	± 0.000	−0.009	−0.006	−0.015	+0.320	+0.327	−0.000	−0.014
STD ^b	0.180	0.187	0.070	0.067	0.102	0.099	0.176	0.183	0.166	0.168
MAE ^c	0.114	0.118	0.060	0.061	0.089	0.091	0.349	0.360	0.118	0.109
MA ^d	0.473	0.497	0.130	0.104	0.175	0.150	0.492	0.479	0.410	0.430

^aMean error.^bStandard deviation.^cMean absolute error.^dMaximum absolute error.^eParameter set 1 (confined AO's).

to a narrow distribution. Couplings are underestimated in all cases, which is in agreement with the behavior observed in set A. SOS-CC2 results in a slightly higher ME of −15 meV and maximum deviation of 54 meV with respect to CC2 couplings.

DFT calculations employing the ω B97X functional result in a ME of +9 meV in case of distances and +4 meV in case of rotation angles. The STD is in the same range as the semi-empirically scaled variants of CC2. For set B, the LC-DFTB method shows slightly increased deviations with respect to CC2. For example, the mean error, STD and maximum error are found to be +28 meV, 29 meV and 90 meV, respectively.

In Figure 9 the behavior of the excitonic couplings is shown for the naphthyridines using CC2 and LC-DFTB. LC-DFTB reproduces the same behavior of the couplings with respect to the distance r as CC2 for nearly all naphthyridines. When comparing the couplings calculated using CC2 in Figure 9, it becomes evident that the strength of the couplings is not strongly dependent on the position of the nitrogen atoms. Both methods show the same behavior qualitatively and quantitatively for nearly all naphthyridines.

3.3 | Dimers in a crystal: Anthracene

As pointed out, the model systems addressed so far only take into account distances and rotation angles. In real crystals, however, there are also varying relative angles of the molecular planes and horizontal translation. These influences are addressed in the following.

3.3.1 | Static crystal dimers

In the anthracene crystal, each molecule couples in three directions with different neighbors. The directions are denoted a , b and c , see Figure 10. In a first step, we compute supermolecular excitonic and Coulomb couplings for one selected dimer along the crystal axes a , b and c , respectively, as extracted from a crystal structure.⁷⁰ Table 8

shows supermolecular excitonic couplings from LC-DFT and LC-DFTB in comparison with LC-DFTB Coulomb couplings. LC-DFT and LC-DFTB values agree quite well for all three directions, the LC-DFT values being slightly larger. From the results of set A data, we expect that LC-DFT slightly overestimates excitonic couplings in acenes. Coulomb couplings, however, are overestimated in the a - and c -directions and underestimated in the b -direction. From the results on the distance dependence as shown above we expect the Coulomb couplings to be slightly too large for long intermolecular separations, where exchange effects can be neglected. This is the case in the a - and c -directions, where intermolecular distances are much larger than in b -direction, which in turn is reflected in the couplings. These differ roughly by an order of magnitude. The smaller values of Coulomb couplings in b -direction most likely result from the neglect of exchange contributions. The difference is about 30%, and this relatively small impact of exchange also along b -direction, where the distance between neighbors is small, is surprising at first sight. To further elucidate this finding, we performed additional calculations on structural models, see Supporting Information-6.

Variations of intermolecular distances and orientations have little impact along the a -direction, while they are sizable along the b -direction. Also, the difference of excitonic and Coulomb couplings is quite large for these variations. Therefore one would expect a larger deviation between these excitonic and Coulomb couplings based on geometrical considerations alone. However, small shifts and tilts of the neighbors in the crystal structure, as visualized in Figure 10, can have a large effect on exchange contributions, thereby reducing their impact. It seems that these molecules are packed in such a way that exchange effects are reduced. Exchange effects are not only important for excitonic couplings, but also for the mutual (Pauli-) repulsion between neighboring molecules. In this light it can be understood that the molecules arrange under the constraint of minimizing exchange repulsion, thereby also reducing the exchange effects in the couplings. Therefore it looks like, although quite surprising, that the Coulomb approximation can be a quite reasonable approach also for such densely packed molecules.

TABLE 7 Excitonic couplings in meV for set B. The values for CC2 are given as absolute coupling strength, while the other methods' results are given relative to the CC2 values

		CC2	ADC(2)	SCS-CC2	SOS-CC2	ω B97X	LC-DFTB ^e		CC2	ADC(2)	SCS-CC2	SOS-CC2	ω B97X	LC-DFTB ^e
1.5-Naphth.	3.5	213	-7	-27	-37	+19	+72	0	73	-4	-8	-21	+12	+49
	4	73	-4	-8	-15	+12	+49	30	16	-3	+1	+1	+5	+48
	5	19	-2	-0	-1	+9	+22	60	2	-1	+2	+3	+3	+22
	6	11	-1	-0	-0	+3	+15	90	0	+0	+0	+0	+1	+0
1.6-Naphth.	3.5	234	-32	-16	-51	-2	+33	0	76	-14	-4	-7	-0	+24
	4	76	-14	-4	-7	-0	+24	30	8	+2	+3	+4	+6	+33
	5	11	+0	+2	+2	+10	+14	60	29	-25	-3	-5	-22	-1
	6	4	+1	+1	+1	+4	+10	90	14	-5	+2	+2	-9	-8
1.7-Naphth.	3.5	213	-4	-40	-54	+20	+58	0	64	-2	-11	-15	+15	+42
	4	64	-2	-11	-15	+15	+42	30	12	-2	-4	-3	+4	+40
	5	11	-1	-1	-1	+15	+17	60	22	-0	-13	-7	-3	+9
	6	5	-1	-0	-1	+3	+11	90	15	-1	-2	-3	-3	-1
1.8-Naphth.	3.5	212	-7	-28	-36	+19	+86	0	72	-4	-8	-9	+14	+55
	4	72	-4	-8	-9	+14	+55	30	14	-3	+1	+10	+6	+48
	5	19	-2	-0	-1	+9	+27	60	1	-0	+0	+9	+1	+11
	6	10	-1	-0	-0	+3	+18	90	1	-0	+0	-1	+1	+3
2.6-Naphth.	3.5	228	-42	-36	-50	-82	+49	0	74	-1	-10	-15	+34	+34
	4	74	-1	-10	-15	+34	+34	30	25	-1	-2	-3	+14	+24
	5	17	-1	-1	-1	+18	+12	60	21	+0	-2	-3	+6	+7
	6	9	-0	-0	-0	+6	+8	90	0	+0	+0	+0	+0	+0
Purin	3.5	185	-11	-31	-43	+48	+90	0	64	-5	-9	-12	+26	+49
	4	64	-5	-9	-12	+26	+49	30	29	-3	-3	-4	+15	+40
	5	19	-2	-1	-2	+34	+19	60	10	-1	+0	+1	+8	+18
	6	11	-1	-1	-1	+7	+13	90	4	+1	-0	-1	+1	+8
Guanin	3.5	215	-20	-27	-50	-10	-48	0	101	-22	-27	-29	-9	-14
	4	101	-22	-27	-29	-9	-14	30	51	-2	-2	-1	+4	+6
	5	27	+0	+1	+1	+10	+6	60	36	-7	-5	-5	-8	-9
	6	16	+1	+1	+1	+6	+5	90	36	-13	-11	-12	-16	+2
ME ^a			-7	-10	-15	+9	+28			-31	-4	-4	+4	+19
STD ^b			10	13	19	21	29			28	7	6	11	21
MAE ^c			7	10	16	16	32			31	4	5	9	22
MA ^d			42	40	54	82	90			101	25	27	34	55

^aMean error.^bStandard deviation.^cMean absolute error.^dMaximum absolute error.^eParameter set 2 (optimized AO's).

3.3.2 | Effect of fluctuations

Having addressed static dimers as extracted from a crystal, in the following the influence of fluctuations in the geometry shall be investigated. Therefore, supermolecular excitonic couplings are calculated for an anthracene dimer in *b*-direction from snapshots of a classical MD simulation of an anthracene crystal, see Section 2.5. Calculations

are performed using LC-DFTB and DFT employing the functional ω B97X. We refrain from using ab-initio methods here, as they are not feasible for such a huge amount of calculations. The performance of LC-DFTB is assessed in comparison to supermolecular couplings and Coulomb couplings, also obtained with LC-DFTB.

In Figure 11 the coupling distributions are shown and the statistical measures can be found in Table 9. The results of the

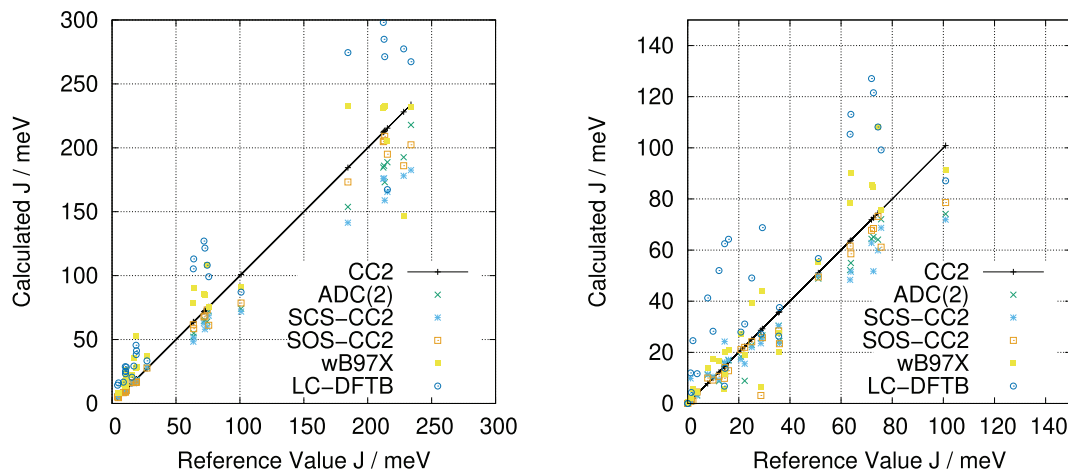


FIGURE 8 Correlation plots of excitonic couplings in case of distances (left) and angles (right) for set B. Note that the plot of the angles has only half the range of the distance plot

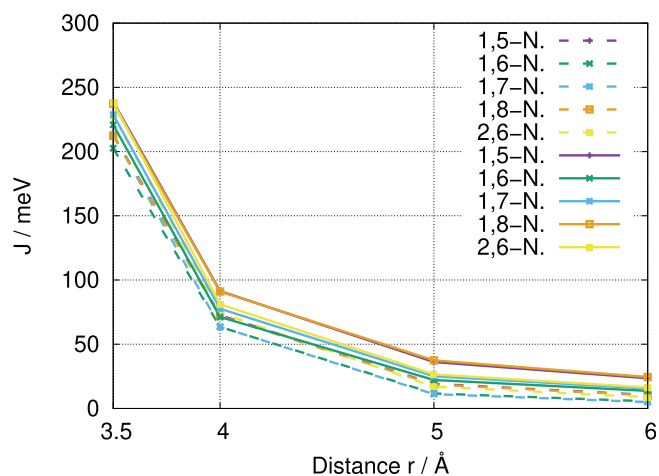


FIGURE 9 Distance dependence of excitonic couplings of different naphthyridine dimers in eV, computed using CC2 (dashed lines) and LC-DFTB (solid lines)

supermolecular approach show increased mean values as well as broader distributions of couplings compared to Coulomb couplings, indicating effects of exchange and overlap are relevant for anthracene in *b*-direction to a certain extent. In section Supporting Information-6.2 we assess aspects of structural fluctuations by considering simple structural variations, showing that exchange effects indeed can become relevant for certain displacements. This explains the broader distributions found for both supermolecular approaches. As discussed for the static case, the LC-DFT couplings are slightly overestimated for anthracene, therefore the whole distribution is slightly shifted to the higher end. Despite the dynamical broadening of the spectrum, the coherence parameter of approximately 0.97 indicates that the transfer can be described by an average coupling, the impact of the fluctuations on transport is therefore small.

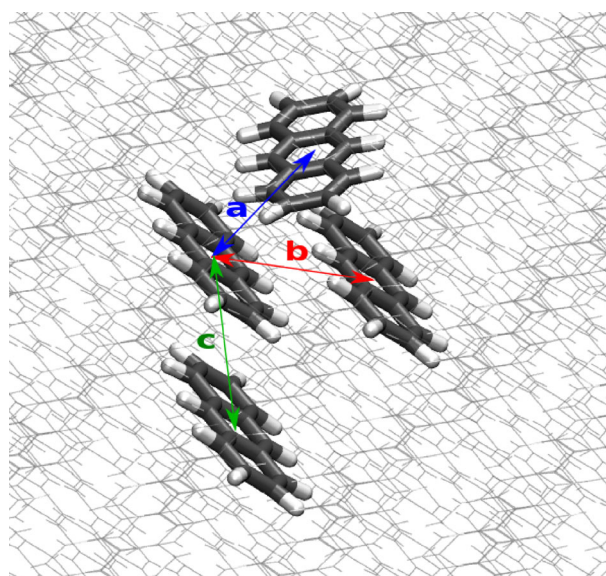


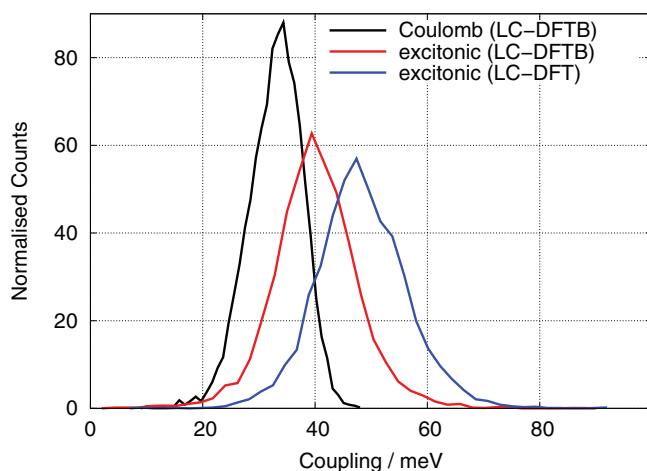
FIGURE 10 Three selected dimers of an anthracene crystal, directions *a*, *b*, *c* highlighted in colors blue, red, and green, respectively

3.3.3 | Influence of excitonic couplings upon diffusion coefficients

To estimate the influence of couplings on the transfer, diffusion constants are calculated using a master equation (MEQ) approach, which is solved for coupling values calculated on the static crystal structure (static) and on the RMS value of sampled structures (dynamic). The latter contains fluctuations of couplings on top of the mean value. Figure 12 shows the time derivative of the exciton MSD, which is directly proportional to the diffusion constant and can be estimated as average of the linear part. The calculated diffusion constants can be found in Table 10. Differences between the values are small and in

TABLE 8 Excitonic couplings in three directions of dimers of an anthracene crystal. All excitonic couplings (J) and Coulomb couplings (J_C) in meV

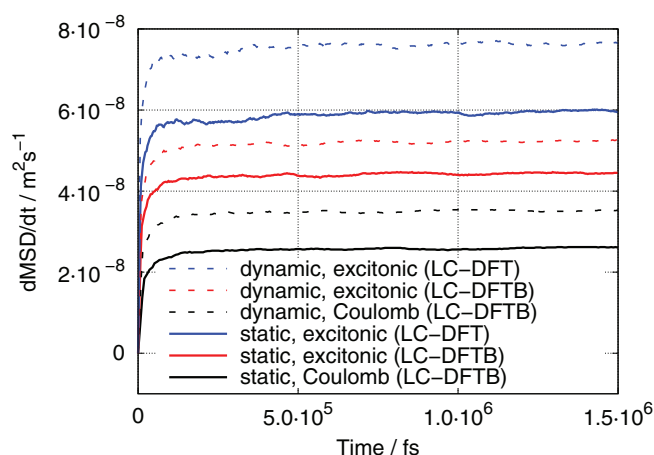
Direction	ω B97X (J)	LC-DFTB ^a (J)	LC-DFTB ^b (J_C)
<i>a</i>	6	4	13
<i>b</i>	43	37	28
<i>c</i>	4	4	6

^aParameter set 1 (confined AO's).^bParameter set 2 (optimized AO's).**FIGURE 11** Histograms of excitonic couplings for sampled structures of an anthracene dimer in *b*-direction calculated with LC-DFTB and LC-DFT (ω B97X) in the conventional supermolecular approach. Additionally, LC-DFTB Coulomb couplings are given**TABLE 9** Analysis of the histograms in Figure 11 in meV

Method	Variant	Mean ^a	STD ^b	RMS ^c	C ^d
LC-DFTB	Coulomb ^e	32	5	33	0.979
	Excitonic ^f	39	8	40	0.963
LC-DFT	Excitonic	47	8	48	0.972

^aMean value.^bStandard deviation.^cRoot mean square, cf. Equation (9).^dCoherence parameter, cf. Equation (10).^eParameter set 1 (confined AO's).^fParameter set 2 (optimized AO's).

agreement with the experimental value of $5 \cdot 10^{-8} \frac{\text{m}^2}{\text{s}}$.⁷⁸ As expected, diffusion is faster with higher values of the couplings. Comparing values obtained by static and dynamic couplings, fluctuations turn out to have a minor impact on diffusion constants, as expected from the estimated coherence parameter. The coupling is therefore mostly defined by the average structure, non-equilibrium structures seem to account for a small additional enhancement of mobility.

**FIGURE 12** Time derivative of the exciton MSD from the MEQ approach for Coulomb and supermolecular excitonic couplings at LC-DFTB and DFT level of theory, calculated on the crystal structure ("static," solid lines) and on the RMS of sampled structures ("dynamic," dashed lines)**TABLE 10** Diffusion constants (in $10^{-8} \frac{\text{m}^2}{\text{s}}$) for exciton transfer along a linear chain of crystal anthracene in *b*-direction calculated with a MEQ approach with static and dynamic (RMS) coupling values. Experimental value is $5 \cdot 10^{-8} \frac{\text{m}^2}{\text{s}}$ ⁷⁸

	Coulomb	Excitonic	
	LC-DFTB	LC-DFTB	LC-DFT
Static	2.6	4.4	5.9
Dynamic	3.5	5.2	7.6

4 | CONCLUSIONS AND OUTLOOK

In this work excitation energies and excitonic couplings for selected acenes, guanine, purine and nitrogen-substituted naphthalenes are investigated. The excitonic couplings are calculated from coupled pairs of excitations as per definition of the Frenkel exciton model. A range of methods from the ab-initio methods CC2 and ADC(2) to the semi-empirical LC-DFTB method are assessed concerning their performance with respect to these couplings. The molecular geometries from the sets A and B, as provided in the Supporting Information, can be used to benchmark other semi-empirical methods employed in energy transport.

While CC2 and ADC(2) exhibit very similar accuracy, in particular for excitonic couplings, the semi-empirically scaled SCS-CC2 and SOS-CC2 result in higher excitation energies. CC2, however, cannot serve as a strict reference for the accuracy of SOS-CC2 and SCS-CC2 as these methods are based on the CC2 reference and thus the scaling leads by definition to a certain deviation.

Results obtained with LC-DFTB depend on the applied parameter set. Absolute excitation energies are in agreement to CC2 when using a parameter set where the DFTB atomic orbital basis set is computed

using a small confinement radius, as usually applied in the DFTB parameterization (parameter set 1). In order to accurately address interactions beyond the short range, such as exchange relevant for supermolecular exciton couplings, more diffuse basis sets have to be used (parameter set 2). With this parameter set, LC-DFTB yields excitonic couplings in agreement with CC2, however, at the cost that absolute excitation energies show increased deviations. This is a clear drawback of minimal basis set methods, requiring different parameterizations, that is, different basis sets for these two applications. Coulomb couplings, computed with the standard basis (set 1), display the correct trend, since in particular for larger distances the Coulomb contribution dominates.

As shown in the present work, Coulomb couplings can also be applied for systems with seemingly small intermolecular distances, if the structures are shifted and tilted in such a way that exchange effects become less important. Nevertheless, DFTB has one significant advantage. While the semi-empirically scaled CC2 variants yield only little computational advantages, DFTB leads to a significantly reduced computation time from hours or days to minutes. We express the hope that the presented couplings will be useful to investigate errors in excitonic couplings computed with other semi-empirical methods for short intermolecular distances as occurring in biological systems or molecular crystals.

ACKNOWLEDGMENTS

This work has been supported by the Deutsche Forschungsgemeinschaft (DFG) through SFB 1249 "N-Heteropolycycles as Functional Materials" (Projects B01, B02, B07). B.M.B. and M.E. acknowledge support by the DFB through the joint grant EL 206/18-1. P.M.D. especially acknowledges Dr. Weiwei Xie for providing his implementation of the master equation approach. The authors acknowledge support by the state of Baden-Württemberg through bwHPC and the German Research Foundation (DFG) through grant no INST 40/575-1 FUGG (JUSTUS 2 cluster).

DATA AVAILABILITY STATEMENT

The data that support the findings of this study are available from the corresponding author upon reasonable request.

ORCID

Marvin Hoffmann  <https://orcid.org/0000-0001-6786-8291>

Andreas Dreuw  <https://orcid.org/0000-0002-5862-5113>

Marcus Elstner  <https://orcid.org/0000-0002-3255-306X>

Sebastian Höfener  <https://orcid.org/0000-0003-4504-347X>

REFERENCES

- [1] S. R. Forrest, *Nature* **2004**, 428, 911.
- [2] J. E. Anthony, *Chem. Rev.* **2006**, 106, 5028.
- [3] S.-S. Sun, L. R. Dalton, *Introduction to Organic Electronic and Optoelectronic Materials and Devices*, CRC Press, Boca Raton **2017**.
- [4] L. Dou, Y. Liu, Z. Hong, G. Li, Y. Yang, *Chem. Rev.* **2015**, 115, 12633.
- [5] Y. Zhao, Y. Guo, Y. Liu, *Adv. Mater.* **2013**, 25, 5372.
- [6] J. Frenkel, *Phys. Rev.* **1931**, 37, 17.
- [7] R. P. Fornari, P. Rowe, D. Padula, A. Troisi, *J. Chem. Theory Comput.* **2017**, 13, 3754.
- [8] C. Curutchet, B. Mennucci, *Chem. Rev.* **2017**, 117, 294.
- [9] K. A. Kistler, F. C. Spano, S. Matsika, *J. Phys. Chem. B* **2013**, 117, 2032.
- [10] A. Muñoz Losa, C. Curutchet, I. F. Galván, B. Mennucci, *J. Chem. Phys.* **2008**, 129, 034104.
- [11] W. Liu, V. Settels, P. H. P. Harbach, A. Dreuw, R. F. Fink, B. Engels, *J. Comput. Chem.* **2011**, 32, 1971.
- [12] E. P. Kenny, I. Kassal, *J. Phys. Chem. B* **2016**, 120, 25.
- [13] A. A. Voityuk, *J. Phys. Chem. C* **2014**, 118, 1478.
- [14] S. A. Mewes, F. Plasser, A. Krylov, A. Dreuw, *J. Chem. Theory Comput.* **2018**, 14, 710.
- [15] J. Aragó, A. Troisi, *Phys. Rev. Lett.* **2015**, 114, 026402.
- [16] J. Aragó, A. Troisi, *J. Chem. Phys.* **2015**, 142, 164107.
- [17] C. Kaufmann, D. Bialas, M. Stolte, F. Würthner, *J. Am. Chem. Soc.* **2018**, 140, 9986.
- [18] A. Kubas, F. Hoffmann, A. Heck, H. Oberhofer, M. Elstner, J. Blumberger, *J. Chem. Phys.* **2014**, 140, 104105.
- [19] A. Kubas, F. Gajdos, A. Heck, H. Oberhofer, M. Elstner, J. Blumberger, *Phys. Chem. Chem. Phys.* **2015**, 17, 14342.
- [20] D. Kánnár, P. G. Szalay, *J. Chem. Theory Comput.* **2014**, 10, 3757.
- [21] J. Almlöf, *Chem. Phys. Lett.* **1991**, 181, 319.
- [22] N. O. C. Winter, C. Hättig, *J. Chem. Phys.* **2011**, 134, 184101.
- [23] N. O. Winter, C. Hättig, *Chem. Phys.* **2012**, 401, 217.
- [24] J. Schirmer, *Phys. Rev. A* **1982**, 26, 2395.
- [25] A. Trofimov, I. Krivdina, J. Weller, J. Schirmer, *Chem. Phys.* **2006**, 329, 1.
- [26] C. Möller, M. S. Plesset, *Phys. Rev.* **1934**, 46, 618.
- [27] P. H. P. Harbach, M. Wormit, A. Dreuw, *J. Chem. Phys.* **2014**, 141, 064113.
- [28] A. Dreuw, M. Wormit, *WIREs Comput. Mol. Sci.* **2015**, 5, 82.
- [29] J. Schirmer, A. B. Trofimov, *J. Chem. Phys.* **2004**, 120, 11449.
- [30] M. Hodecker, D. R. Rehn, A. Dreuw, S. Höfener, *J. Chem. Phys.* **2019**, 150, 164125.
- [31] M. Wormit, D. R. Rehn, P. H. Harbach, J. Wenzel, C. M. Krauter, E. Epifanovsky, A. Dreuw, *Mol. Phys.* **2014**, 112, 774.
- [32] C. Adamo, D. Jacquemin, *Chem. Soc. Rev.* **2013**, 42, 845.
- [33] D. J. Tozer, R. D. Amos, N. C. Handy, B. O. Roos, L. Serrano-Andres, *Mol. Phys.* **1999**, 97, 859.
- [34] A. Dreuw, M. Head-Gordon, *Chem. Rev.* **2005**, 105, 4009.
- [35] R. Bauernschmitt, R. Ahlrichs, *Chem. Phys. Lett.* **1996**, 256, 454.
- [36] A. Dreuw, J. L. Weisman, M. Head-Gordon, *J. Chem. Phys.* **2003**, 119, 2943.
- [37] A. Dreuw, M. Head-Gordon, *J. Am. Chem. Soc.* **2004**, 126, 4007.
- [38] B. Champagne, E. A. Perpète, S. J. A. van Gisbergen, E. J. Baerends, J. D. Snijders, C. Soubra-Ghauoi, K. A. Robins, B. Kirtman, *J. Chem. Phys.* **1998**, 109, 10489.
- [39] S. J. A. van Gisbergen, P. R. T. Schipper, O. V. Gritsenko, E. J. Baerends, J. D. Snijders, B. Champagne, B. Kirtman, *Phys. Rev. Lett.* **1999**, 83, 694.
- [40] P. L. de Boei, F. Kootstra, J. A. Berger, R. van Leeuwen, J. G. Snijders, *J. Chem. Phys.* **2001**, 115, 1995.
- [41] J. Plötnner, D. J. Tozer, A. Dreuw, *J. Chem. Theory Comput.* **2010**, 6, 2315.
- [42] M. M. Mikołajczyk, R. Zaleśny, Ż. Czyżnikowska, P. Toman, J. Leszczynski, W. Bartkowiak, *J. Mol. Model.* **2011**, 17, 2143.
- [43] J.-C. Lee, J.-D. Chai, S.-T. Lin, *RSC Adv.* **2015**, 5, 101370.
- [44] G. Seifert, D. Porezag, T. Frauenheim, *Int. J. Quantum Chem.* **1996**, 58, 185.
- [45] M. Elstner, D. Porezag, G. Jungnickel, J. Elsner, M. Haugk, T. Frauenheim, S. Suhai, G. Seifert, *Phys. Rev. B: Condens. Matter Mater. Phys.* **1998**, 58, 7260.
- [46] M. Elstner, G. Seifert, *Philos. Trans. R. Soc. A* **2014**, 372, 20120483.
- [47] V. Lutsker, B. Aradi, T. A. Niehaus, *J. Chem. Phys.* **2015**, 143, 184107.
- [48] J. J. Kranz, M. Elstner, B. Aradi, T. Frauenheim, V. Lutsker, A. D. Garcia, T. A. Niehaus, *J. Chem. Theory Comput.* **2017**, 13, 1737.

- [49] P.-A. Plötz, T. Niehaus, O. Kühn, *J. Chem. Phys.* **2014**, *140*, 174101.
- [50] J. J. Kranz, M. Elstner, *J. Chem. Theory Comput.* **2016**, *12*, 4209.
- [51] Z.-Q. You, C.-P. Hsu, G. R. Fleming, *J. Chem. Phys.* **2006**, *124*, 044506.
- [52] Z.-Q. You, C.-P. Hsu, *J. Chem. Phys.* **2010**, *133*, 074105.
- [53] R. D. Harcourt, G. D. Scholes, K. P. Giggino, *J. Chem. Phys.* **1994**, *101*, 10521.
- [54] C. Ye, L. Zhou, X. Wang, Z. Liang, *Phys. Chem. Chem. Phys.* **2016**, *18*, 10818.
- [55] D. A. Hartzler, L. V. Slipchenko, S. Savikhin, *J. Phys. Chem. A* **2018**, *122*, 6713.
- [56] H. Koch, O. Christiansen, P. Jorgensen, J. Olsen, *Chem. Phys. Lett.* **1995**, *244*, 75.
- [57] M. Schreiber, M. R. Silva-Junior, S. P. A. Sauer, W. Thiel, *J. Chem. Phys.* **2008**, *128*, 134110.
- [58] D. Jacquemin, V. Wathelet, E. A. Perpète, C. Adamo, *J. Chem. Theory Comput.* **2009**, *5*, 2420.
- [59] A. D. Laurent, D. Jacquemin, *Int. J. Quantum Chem.* **2013**, *113*, 2019.
- [60] R. Send, M. Kühn, F. Furche, *J. Chem. Theory Comput.* **2011**, *7*, 2376.
- [61] R. J. Cave, M. D. Newton, *Chem. Phys. Lett.* **1996**, *249*, 15.
- [62] R. J. Cave, M. D. Newton, *J. Chem. Phys.* **1997**, *106*, 9213.
- [63] TURBOMOLE, a development of University of Karlsruhe and Forschungszentrum Karlsruhe GmbH, 1989-2007, TURBOMOLE GmbH, since 2007. Karlsruhe, Germany. <http://www.turbomole.com>.
- [64] O. Treutler, R. Ahlrichs, *J. Chem. Phys.* **1995**, *102*, 346.
- [65] M. Von Arnim, R. Ahlrichs, *J. Comput. Chem.* **1998**, *19*, 1746.
- [66] Y. Shao, Z. Gan, E. Epifanovsky, A. T. B. Gilbert, M. Wormit, J. Kussmann, A. W. Lange, A. Behn, J. Deng, X. Feng, D. Ghosh, M. Goldey, P. R. Horn, L. D. Jacobson, I. Kaliman, R. Z. Khaliullin, T. Kuš, A. Landau, J. Liu, E. I. Proynov, Y. M. Rhee, R. M. Richard, M. A. Rohrdanz, R. P. Steele, E. J. Sundstrom, H. L. Woodcock III, P. M. Zimmerman, D. Zuev, B. Albrecht, E. Alguire, B. Austin, G. J. O. Beran, Y. A. Bernard, E. Berquist, K. Brandhorst, K. B. Bravaya, S. T. Brown, D. Casanova, C. M. Chang, Y. Chen, S. H. Chien, K. D. Closser, D. L. Crittenden, M. Didenhofen, R. A. DiStasio Jr., H. Do, A. D. Dutoi, R. G. Edgar, S. Fatehi, L. Fusti-Molnar, A. Ghysels, A. Golubeva-Zadorozhnaya, J. Gomes, M. W. D. Hanson-Heine, P. H. P. Harbach, A. W. Hauser, E. G. Hohenstein, Z. C. Holden, T. C. Jagau, H. Ji, B. Kaduk, K. Khistyayev, J. Kim, J. Kim, R. A. King, P. Klunzinger, D. Kosenkov, T. Kowalczyk, C. M. Krauter, K. U. Lao, A. D. Laurent, K. V. Lawler, S. V. Levchenko, C. Y. Lin, F. Liu, E. Livshits, R. C. Lochan, A. Luenser, P. Manohar, S. F. Manzer, S. P. Mao, N. Mardirossian, A. V. Marenich, S. A. Maurer, N. J. Mayhall, E. Neuscamman, C. M. Oana, R. Olivares-Amaya, D. P. O'Neill, J. A. Parkhill, T. M. Perrine, R. Peverati, A. Prociuk, D. R. Rehn, E. Rosta, N. J. Russ, S. M. Sharada, S. Sharma, D. W. Small, A. Sodt, T. Stein, D. Stück, Y. C. Su, A. J. W. Thom, T. Tsuchimochi, V. Vanovschi, L. Vogt, O. Vydrov, T. Wang, M. A. Watson, J. Wenzel, A. White, C. F. Williams, J. Yang, S. Yeganeh, S. R. Yost, Z. Q. You, I. Y. Zhang, X. Zhang, Y. Zhao, B. R. Brooks, G. K. L. Chan, D. M. Chipman, C. J. Cramer, W. A. Goddard III, M. S. Gordon, W. J. Hehre, A. Klamt, H. F. Schaefer III, M. W. Schmidt, C. D. Sherrill, D. G. Truhlar, A. Warshel, X. Xu, A. Aspuru-Guzik, R. Baer, A. T. Bell, N. A. Besley, J. D. Chai, A. Dreuw, B. D. Dunietz, T. R. Furlani, S. R. Gwaltney, C. P. Hsu, Y. Jung, J. Kong, D. S. Lambrecht, W. Z. Liang, C. Ochsenfeld, V. A. Rassolov, L. V. Slipchenko, J. E. Subotnik, T. van Voorhis, J. M. Herbert, A. I. Krylov, P. M. W. Gill, M. Head-Gordon, *Mol. Phys.* **2015**, *113*, 184.
- [67] F. Neese, *Wiley Interdiscip. Rev. Comput. Mol. Sci.* **2018**, *8*, 4.
- [68] R. Baer, D. Neuhauser, *Phys. Rev. Lett.* **2005**, *94*, 2.
- [69] E. Livshits, R. Baer, *Phys. Chem. Chem. Phys.* **2007**, *9*, 2932.
- [70] M. Krämer, P. M. Dohmen, W. Xie, D. Holub, A. S. Christensen, M. Elstner, *J. Chem. Theory Comput.* **2020**, *16*, 4061.
- [71] W. Young, E. Elcock, *Proc. Phys. Soc.* **1966**, *89*, 735.
- [72] H. Oberhofer, K. Reuter, J. Blumberger, *Chem. Rev.* **2017**, *117*, 10319.
- [73] R. A. Marcus, *J. Chem. Phys.* **1956**, *24*, 966.
- [74] R. A. Marcus, *Rev. Mod. Phys.* **1993**, *65*, 599.
- [75] I. A. Balabin, J. N. Onuchic, *Science* **2000**, *290*, 114.
- [76] I. A. Balabin, D. N. Beratan, S. S. Skourtis, *Phys. Rev. Lett.* **2008**, *101*, 158102.
- [77] A. Heck, J. J. Kranz, T. Kubař, M. Elstner, *J. Chem. Theory Comput.* **2015**, *11*, 5068.
- [78] J. S. Meth, C. Marshall, M. Fayer, *Solid State Commun.* **1990**, *74*, 281.

SUPPORTING INFORMATION

Additional supporting information may be found online in the Supporting Information section at the end of this article.

How to cite this article: N. Schieschke, B. M. Bold, P. M. Dohmen, D. Wehl, M. Hoffmann, A. Dreuw, M. Elstner, S. Höfener, *J Comput Chem* **2021**, *42*(20), 1402. <https://doi.org/10.1002/jcc.26552>